



Trans. Nonferrous Met. Soc. China 30(2020) 1058-1070

Transactions of **Nonferrous Metal Society of China** 

www.tnmsc.cn



### Manganese potential mapping in western Guangxi-southeastern Yunnan (China) via spatial analysis and modal-adaptive prospectivity modeling

Fan-yun WANG<sup>1,2</sup>, Xian-cheng MAO<sup>1</sup>, Hao DENG<sup>1</sup>, Bao-yi ZHANG<sup>1</sup>

1. Key Laboratory of Metallogenic Prediction of Nonferrous Metals of Ministry of Education, School of Geosciences and Info-Physics, Central South University, Changsha 410083, China;

2. Central South University Press, Changsha 410083, China

Received 20 November 2019; accepted 28 March 2020

Abstract: While the region of western Guangxi-southeastern Yunan, China, is known and considered prospective for manganese deposits, carrying out prospectivity mapping in this region is challenging due to the diversity of geological factors, the complexity of geological process and the asymmetry of geo-information. In this work, the manganese potential mapping for further exploration targeting is implemented via spatial analysis and modal-adaptive prospectivity modeling. On the basis of targeting criteria developed by the mineral system approach, the spatial analysis is leveraged to extract the predictor variables to identify features of the geological process. Specifically, a metallogenic field analysis approach is proposed to extract metallogenic information that quantifies the regional impacts of the synsedimentary faults and sedimentary basins. In the integration of the extracted predictor variables, a modal-adaptive prospectivity model is built, which allows to adapt different data availability and geological process. The resulting prospective areas of high potential not only correspond to the areas of known manganese deposits but also provide a number of favorable targets in the region for future mineral exploration.

Key words: prospectivity mapping; manganese deposit; western Guangxi-southeastern Yunnan; field analysis approach; modal-adaptive prospectivity modeling

#### 1 Introduction

As a result of the fast-developing industry in China, China becomes the largest consumer of manganese (Mn) ore resources. To meet the increasing demands, the prospectivity of new Mn resources becomes an urgent requirement. On the other hand, China is the 5th largest country for the total reserves of Mn resources all over the world [1,2]. The Mn deposits in China occur mainly in the margins of platforms. The margin of the Yangtze Block corresponds to the most significant Mn metallogenic zone of China, which is located in Guangxi, Hunan, Guizhou and Yunnan provinces. Specifically, the region of western Guangxisoutheastern Yunan (WGSY) accumulates more than 30% of the total Mn reserves of China. Regarding to the presence of the super-large Mn deposits such as Xialei and the other significant deposits in the western Guangxi-southeastern Yunan, China, other locations within this region are considered prospective for Mn mineralization due similar geological, lithofacies paleogeography settings. Therefore, mapping Mn potential and delineation of prospective areas for further investigations and explorations in this region may assist in increasing the Mn reserves in China [3,4].

Recently, due to the capabilities of quantitatively assessing geological evidence and objective assigning priorities to exploration, the GIS-based

Foundation item: Project (2017YFC0601503) supported by the National Key R&D Program of China; Projects (41772349, 41972309, 41472301, 41772348) supported by the National Natural Science Foundation of China

Corresponding author: Hao DENG; E-mail: haodeng@csu.edu.cn

DOI: 10.1016/S1003-6326(20)65277-3

prospectivity mapping has become the mainstream technique in exploration targeting [5–12]. Focused on identifying areas with strong likelihoods of mineralization, the techniques of GIS-based prospectivity mapping generally contain an integrated analysis of targeting criteria with the guidance of prior geological knowledge, which provides an effective way to combine the geological data into a single prospectivity map [13].

When coming to the regional-scale area of WGSY, however, existing GIS-based prospectivity approaches face great challenges in mapping Mn potential in the area. Firstly, the genesis of the Mn deposits refers to a variety of metallogenic factors including structures, stratums, lithofacies and paleogeography [14,15]. Given such a large number of geological factors, it is essential to develop available and effective targeting criteria and predictor variables to constrain the prospectivity mapping. Specifically, a problem has been raised on how to extract predictor variables indicative of Mn mineralization from the existing geological data. For instance, while many Mn deposits are controlled by the multiple sedimentary faults and the control is attenuated progressively with the increasing distance to the faults, simply using conventional spatial analysis techniques such as the buffer analysis is limited in representing such a spatially superposed and attenuated control. Thus, an additional spatial analysis approach should be developed and applied to the geological objects such that the cryptic metallogenic information to indicate mineralization can be exposed. Secondly, due to difficulty in obtaining all of the datasets for geological factors covering the entire region and the spatial variability in geological process and metallogenic condition, the issue of information asymmetry is posed in the prospective modeling. Thus, the prospectivity modeling is required to integrate different predictor variables in a modal-adaptive fashion such that different data collections and various geological processes in the region can be taken into full consideration in Mn prospectivity.

In this contribution, we propose a novel GIS-based prospectivity framework tailored for Mn potential mapping in the WGSY region. To develop targeting criteria from a variety of geological factors and data associated with Mn deposits, the mineral system approach is applied regarding to the

mineral source, transport, trap and deposition. To extract indicative predictor variables corresponding to the targeting criteria, the metallogenic field analysis is presented as a spatial analysis method allowing to provide deep insights into underlying metallogenic control to the Mn deposit. And to handle the information asymmetry in prospective modeling, a modal-adaptive prospectivity modeling method is proposed to adapt different combinations of predictor variables attributed to different data collections and geological processes in the region. The final prospectivity results demonstrate that the proposed prospectivity frameworks are well-suited in addressing the issues raised in Mn potential mapping in the WGSY region.

#### 2 Geological setting and mineral deposits

The study area covers the southwest of Guangxi to the east of Yunnan Province, from Xuanwei–Guangnan and Guangxi Bama in the north to the China–Vietnam border in the south, to the Pingguo–Longan area in Guangxi in the east, and to Kaiyuan–Mengzi in the west. The geographic coordinates range in 103.5°–107.5° east longitude and 22.67°–26.5° north latitude, covering an area of about 40000 km<sup>2</sup>.

The study area (Fig. 1), located in the southwestern margin of the Yangtze platform, contains the southwestern Guangxi Mn ore concentration area and the southestern Yunnan Mn ore concentration area. The southwestern Guangxi Mn ore concentration area is located in the southwest of the Nanhua platform-Youjiang reclaimed geosyncline. The third-order tectonic units include the Guangxi West Depression, the Jingxi-Tiandong Uplift, and the Xialei-Lingma Depression. The strata can be roughly divided into three major sets in the study area, namely the pre-Devonian basement system, the cover rock series dominated by the Late Paleozoic to the Middle Triassic marine deposits, and the Cenozoic hawthorn facies river facies and lacustrine facies. According to the lithological sequence characteristics of Mn-bearing formations, tectonic environment and geochemical characteristics during the formation, Mn-bearing rock series in this area can be divided into two types: Mn-bearing siliceous limestone series and Mn-bearing carbonate series [14]. On the

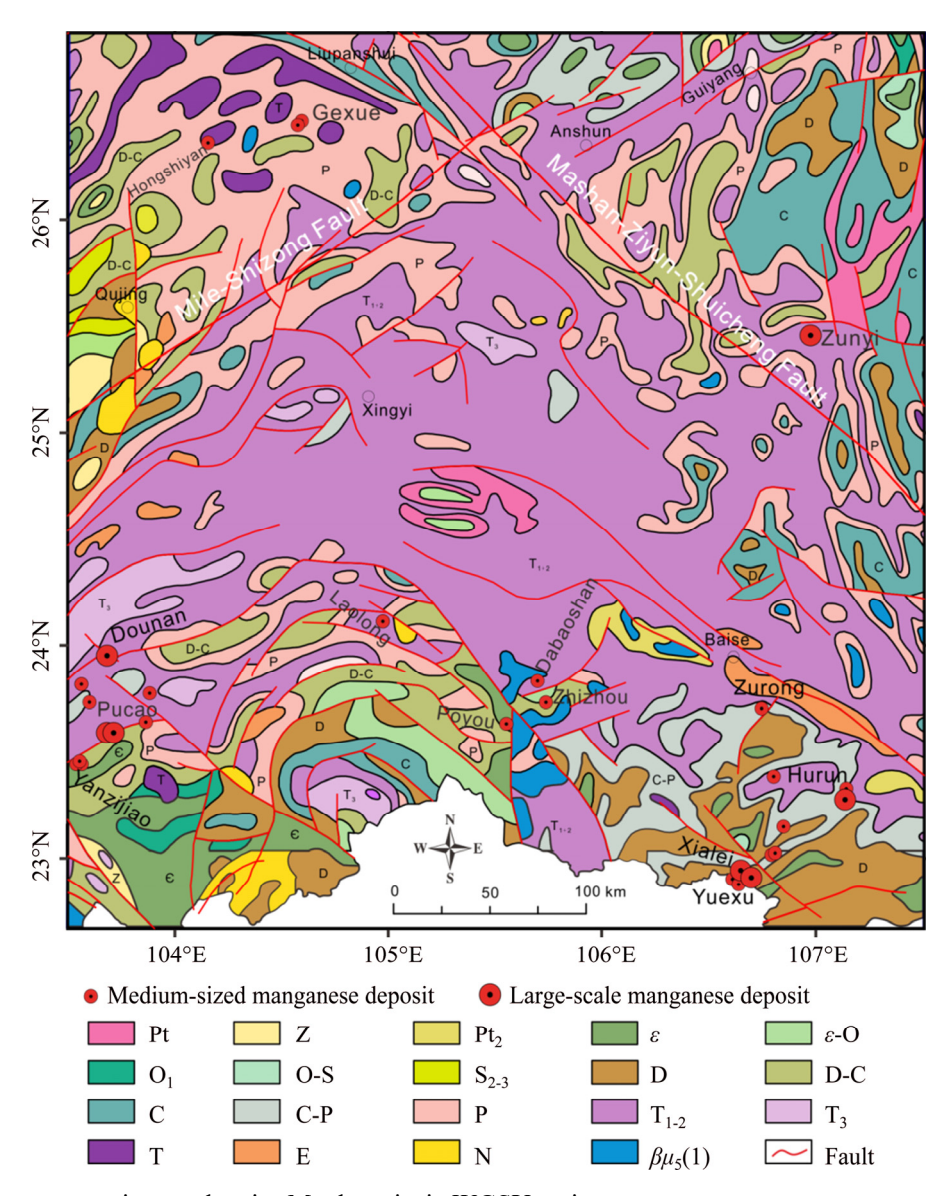


Fig. 1 Geologic map superimposed major Mn deposits in WGSY region

other hand, the southeastern Yunnan Mn ore concentration area is located in the southeastern fold belt of the South China fold system, its northern and western parts are respectively adjacent to the Yangtze platy belt and the Ailaoshan fault block of the Yangtze River, and they are bounded by the Maitreya-Shizong fault and the Honghe fault. The northern part of the strata in the area is dominated by the Mesozoic, the southern part is dominated by the Paleozoic and generally bounded by the near EW fault. The Triassic of Mesozoic is mainly distributed in the regional syncline axis and Xichou-Malipo area of northeastrn Wenshan-Malipo fault, in which two main types of Mn-bearing rock series are discovered in the area: Mn-bearing clastic rock series (Dounan style) and

Mn-bearing carbonate series (Baixian style) [15].

There are more than 200 Mn deposits (points) discovered in WGSY region [16], which includes famous Mn deposits such as Xialei and Dounan. The evolution of Mn deposits in the study area is controlled by the tectonic evolution of the southern continental paleocontinent while dominated by the environment of the marginal sea and the Mn-bearing basin [17]. The main metallogenic factors controlling the formation and distribution of Mn deposit contain the nature of the Mn-bearing sedimentary basin and its tectonic conditions, metallogenic age, stratigraphic horizon, sedimentary formation, mineral superimposed and enrichment conditions, and supergene enrichment conditions [18].

## 3 Conceptual exploration model based on mineral system approach

As there exist multiple geological factors concluded by previous researchers, to develop a set of available predictor variables as proxies for the ore-forming process and thus to constrain the modeling of Mn prospectivity are still challenging. Here, we use a mineral system approach to guide the identification of targeting criteria and thus to build Mn prospective models in the study area. Defining a mineral system requires several key geological components [19-23]: a source of energy that drives the system; sources of fluids, metals and ligands; pathways along which fluids can migrate to trap zones; a trap zone where fluid flow can be focused and its composition modified; and outflow zones for discharge of the residual fluid. Since the mineral system approach is based on a geological process in contrast to traditional ore deposit models, it focuses on a similar process in the mineral system rather than a specific geological setting and metallogenic type. Thus, the mineral system approach is scalable to multiple deposit styles [24] in the WGSY region while considering the difference among the deposits.

#### 3.1 Source of energy and metals

The Mn deposits in WGSY region were a consequence of Rodinia supercontinent cleavage. During the continental break-up process, a large number of syngenetic faults were formed. As a result, the source material of Mn was brought into the sedimentary basins through hydrothermal exhalative process, which caused mineralization in a stable period of this process [4]. Thus, the Mn deposits were controlled by the configuration of synsedimentary structures. Here, the synsedimentary faults were taken as the spatial proxies for the source of energy and metals in the hydrothermal exhalative process. Moreover, in the secondary enrichment of metals resulted from weathering, leaching, and accumulation process, the primary sedimentary strata acted as the source beds. To reflect the source of metals in the secondary enrichment of Mn, the thickness of Mn sedimentary strata was adopted to represent the Mn content of the source beds.

#### 3.2 Transport to trap

WGSY region is under the background of structural tension, which leads to the forming of a marginal rift basin in a shallow sea. Due to the strong convection of the hot water at the bottom of the basin during the continental break-up process, the deep Mn materials were brought into a basin [14]. With the Mn-bearing materials, the transport to trap also requires a favorable basin environment that allows Mn materials to migrate to traps. The structurally stable extensional basins not only link to the Mn source, but also drive the migration of Mn materials to traps and the secondary enrichment of Mn. Notably, the Mnbearing fluids tend to ponder in the basin margin. The area of a large geothermal gradient in the rift basin and the faster thermal cycle in the late stage sedimentary is especially favored sedimentary of the Mn-bearing materials [1]. Additionally, since the Mn deposit is concentrated on limited sedimentary strata, the sedimentary strata reflect the timing of migration and sedimentary [25]. As such, sedimentary basins and sedimentary strata are mapped as the proxies reflecting the transport and sedimentary process.

#### 3.3 Formation of trap and deposition of metals

With rich Mn materials, the trap and formation of Mn ores require a favorable environment such as tranquil deep-water basins. Thus, the Mn deposit was related to the sedimentary faces and lithofacies. Additionally, most of Mn deposits in the study area were caused by primary enrichment of Mn in submarine sedimentary, in which the Mn-bearing fluids were constrained by the topology of paleo-seafloor such as depression. In the secondary enrichment of Mn, the oxidation and preservation of Mn metals were also related to surficial topology [26]. The type of the trap and enrichment of Mn are impacted and reflected by the lithology of the sedimentary strata. In the primary enrichment, due to the marine sedimentary, the favorable environment for Mn deposition is featured by siliceous and mudstone. In the secondary enrichment, due to the weathering process, different lithologies of primary Mn mineralization have inconsistent physicochemical properties, resulting in different trap and deposition types. Finally, the deposition of an economic quantity of metals in the mineralization system was also impacted by the

factors for the formation of the trap, which can be reflected in aeromagnetic anomalies.

Overall, for each mineral system element, the developed targeting criteria are summarized in Table 1, which also lists the spatial proxies of the targeting criteria and available dataset to derive the predictor variables.

#### 4 Spatial analysis and predictor variables

#### 4.1 Spatial analysis method

#### 4.1.1 Motivation

While the sedimentary faults and sedimentary basins are deemed as the targeting criteria corresponding to the source and transport elements in the mineral system, their metallogenic control is non-trivial to quantify on account of the complex correlation to the Mn deposits, which can be reflected in the following two aspects [26].

- (1) The metallogenic control of synsedimentary faults is attenuated gradually with the increasing distance to the faults. And the metallogenic control of different synsedimentary faults has a superposition effect on the Mn metallogenesis. In other words, the distribution of Mn deposits is not only related to the distance to the synsedimentary faults, but also affected by the superposed control of multiple fractures. This is reflected by the fact that Mn resources are more concentrated in the vicinity of the intersection of synsedimentary faults.
  - (2) The metallogenic control of sedimentary

basins is also attenuated gradually with the increasing distance to the basin margin. But the metallogenic control of sedimentary basins does not show the superposition effect, that is, the Mn deposits are distributed within the sedimentary basins or within a certain distance out of the basins.

To represent the above correlations, the traditional spatial analysis such as buffer analysis can be used to express the spatial correlation by identifying the proximity domain of the geological objects. Since the traditional buffer analysis is capable of extracting the control domain of the associated geological factors, the inability to represent the controlling magnitude limits the buffer analysis in reflecting the attenuated and superposed control of the geological objects such as the sedimentary basins and synsedimentary faults. Moreover, carrying out the metallogenic geodynamical simulation [27] is also computational intractable in such a large study area. Therefore, to represent the superposed control of synsedimentary faults, we propose the metallogenic control filed that reflects the control of regional structure-magma-hydrothermal processes via the synsedimentary faults. On the other hand, we adopted a distance field to represent the spatially attenuated control of the sedimentary basins.

#### 4.1.2 Metallogenic control field

Since the jects and sprays of the submarine deep post-magmatic hot brine (including Mn, iron and other components) in the vicinity of synsedimentary faults provide a mass of Mn materials

Table 1 Targeting criteria and predictor variables derived from mineral system approach for Mn deposits in WGSY region

Component	Targeting criterion	Primary data	Predictor variable
Source	Spatial relation to synsedimentary faults	Geological mapping	Control field of synsedimentary faults
	Mn-rich sedimentary strata	Sedimentary-faces and paleogeography mapping	Thickness of sedimentary strata
Transport	Proximity to the margin of Sedimentary basins	Sedimentary structural interpretation and mapping	Distance field of basin margins
	Sedimentary timings	Sedimentary-faces and paleogeography mapping	Stratum code
Trap and deposition	Lithofacies	Sedimentary-faces and paleogeography mapping	Lithofacies code
	Paleo-seafloor topology	Digital elevation models	Topological erosion degree
	Lithology	Sedimentary-faces and paleogeography mapping	Lithology code
	Metal disposition	Geophysical mapping	Aeromagnetic anomalies values

and the energy for mass transfer, the mass and heat diffusion through the synsedimentary faults are deemed to be critical for Mn transport and enrichment. Here, the control of the synsedimentary faults is represented by the diffusion equation that describes the distribution of the heat in the diffusion process and the evolution of the concentration of mineralization materials. Generally, the diffusion equation treats the problems in which the component concentration and temperature vary both with spatial position and time, i.e., C(x,t), where  $x \in \mathbb{R}^3$  denotes the position and t denotes the time. According to the Fick's second law and the heat diffusion equation, both the concentration and temperature can be described by the partial differential equation of the form:

$$\frac{\partial C}{\partial t} = D\nabla^2 C \tag{1}$$

where D is the diffusion coefficient and  $\nabla^2$  denotes the Laplacian operator. Given the equation in Eq. (1), we seek the steady-state solution by regarding component concentration and temperature as independent of time, that is, reach a steady state. Thus, Eq. (1) is reduced to the Laplace's equation as

$$\nabla^2 C = 0 \tag{2}$$

Another benefit of solving Laplace's equation in Eq. (2) instead of the original equation in Eq. (1) is that the velocity potential of fluid field satisfies Laplace's equation, which means that the solution also represents the potential flow of the fluids in a submarine and thus further reflects the structure-magma control to the mineralization.

Equation (2) can be solved by setting up certain boundary conditions. In our scenario, the synsedimentary faults are regarded as the boundary with high component concentration and temperature, whereas the outer boundary of the research region is set as background centration and normal temperature. By setting up the boundary conditions, Eq. (2) can be solved by using the numeric method. In practice, the finite element method is used to solve Eq. (2), which is implemented by MATLAB PDE toolbox [28].

#### 4.1.3 Euclidean distance field

To represent the metallogenic controlling effect all over the region, each point in the metallogenic distance field is assigned the shortest distance to the target geological objects. Here, the Euclidean distance is chosen as the distance metric. Given that the space is discretized into multiple cells, we can calculate the distance field all over the set of pixels efficiently by using Euclidean distance transform [29], which exploits the spatial coherence of the shortest distance in neighboring pixels to speed up the calculation. However, the Euclidean distance transform assumes a discretization of the space, which will lead to an approximated solution of the distance field. Instead, we calculate the accurate distance field for the geological object.

To calculate the accurate distance field, we focus on the shortest distance to the cases of line and area geological objects, whereas the case of point objects is the trivial point—point distance. Since the line and area objects are represented by polylines and polygons respectively in practice, calculating the shortest distance to both types of the objects can be decomposed into the calculation of the shortest distance to each line segment composed of the polyline or the polygon. For the sake of simplicity, let us take a polygon P composed of P vertices  $\{v_1, \dots, v_n\}$  as an example. Given a point P, the shortest distance P0 from P1 to P2 can be formulated as follows:

$$d(p,P) = \min\{d(p,\overline{v_1v_2}),\cdots,d(p,\overline{v_{n-1}v_n}),d(p,\overline{v_{n-1}v_0})\}$$
(3)

where  $d(p, \overline{v_l v_{l+1}})$  denotes the shortest distance between p and line segment  $\overline{v_l v_{l+1}}$ .

#### 4.2 Predictor variables

The predictor variables outlined below are derived from the conceptual exploration model based on mineral system approach (Table 1). And the critical predictor variables such as the control of synsedimentary faults and synsedimentary basins, which represent source and transport process respectively, are extracted by the spatial analysis method described in Subsection 4.1.

4.2.1 Predictor maps representing metal sources

#### 4.2.1.1 Control field of synsedimentary faults

In the southeastern Yunnan, the Middle Triassic Latin Nickel period is a relatively active sedimentary tectonic setting. The fault activity is closely related to mineralization. The ore-forming materials are mainly derived from deep hydrothermal fluids, which are deep-water deep-source hydrothermal deposition in the paleocontinental rift environment. The ore belt is controlled by a linear

structure, and the sub-belt is controlled by a composite structure of linear intersection. On the other hand, there are two parallel NE-oriented sedimentary strike-slip faults in the southwestern Guangxi, namely the Xialei-Dongping Tongsheng strike-slip fault and the Longbang-Dizhou Tongsheng strike-slip fault, which are slipping structures controlling the Mn deposits in Late Devonian. Thus, Late Devonian synsedimentary faults and Middle Triassic synsedimentary faults are considered to be significant to the Mn mineralization. As such, we calculate metallogenic control field for the two types of synsedimentary faults, resulting in the Late Devonian synsedimentary fault control field fF D3 and the Middle Triassic synsedimentary fault control field fF T2 (Fig. 2).

#### 4.2.1.2 Thickness of sedimentary strata

The sedimentary thickness of strata is considered as the other type of predictor variable representing the sourcing process. According to the formation time of sedimentary strata, sedimentary thickness of strata in the study area refers to (1) the Middle Devonian Eifelian sedimentary thickness g(HAF D2), (2) the Late Frasian sedimentary Devonian thickness g(HFL D3), (3) the Late Devonian Famennian sedimentary thickness g(HFM D3), and (4) the Middle Triassic falang formation sedimentary thickness g(H T2f).

### 4.2.2 Predictor maps representing metal transport 4.2.2.1 Distance field of basin margins

The sedimentary of Mn deposites requires a basin environment with low-energy and quite

deep-water that allows the Mn-bearing fluids to migrate to trap zones. Thus, the ore-control of the Mn-bearing basin is related to the distance to the margin of the basins, which is represented by the Euclidean distance field. The Mn-forming age of the study area is concentrated, mainly involving Middle Devonian. Late Devonian. Carboniferous, Early Triassic, and Middle Triassic, etc. Accordingly, we calculate the Euclidean distance field for sedimentary basins including: (1) the Late Devonian deep-water basin distance field dPSS D3, (2) the Early Triassic turbidity basin distance field dPZL T1, (3) the Early Triassic shallow-water platform distance field dPQS T1, and (4) the Middle Triassic deep-water basin distance field dPSS T2. Figure 3 shows the above evidence layers for the sedimentary basin.

#### 4.2.2.2 Stratum code

The Mn deposits in western Guangxi-southeastern Yunnan are generally formed in the Late Devonian, the Early Carboniferous Tatang and the Early Triassic. To build the quantitative relation to the strata, each stratum is assigned to a numeric code. Figure 3 illustrates the spatial distribution of the strata.

4.2.3 Predictor maps representing Mn trap and deposition

#### 4.2.3.1 Lithofacies code

Sedimentary facies and lithofacies are taken as the proxies for the metal trap and deposition. According to the metallogenic stages, the sedimentary facies in different stages in WGSY region are considered, which correspond to six predictor variables: (1) the Middle Devonian Eifelian

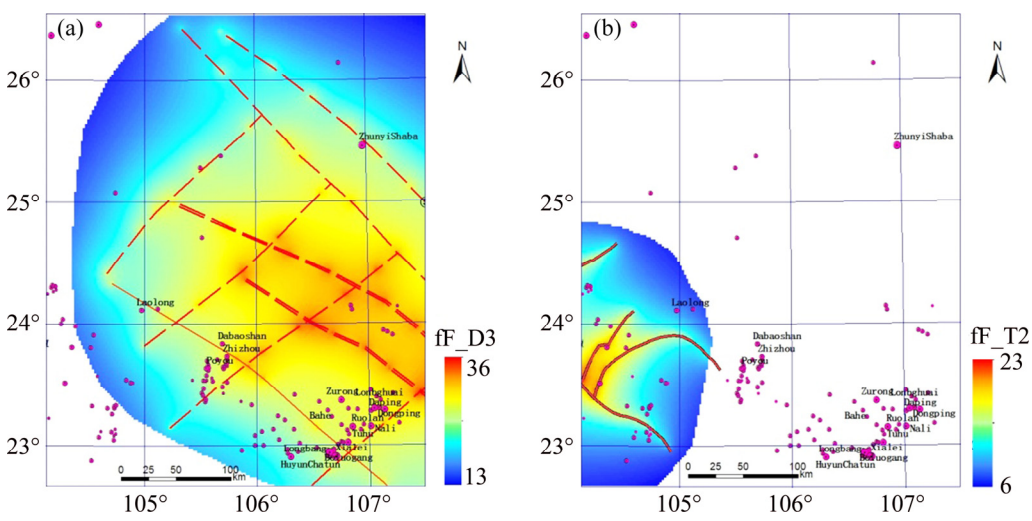
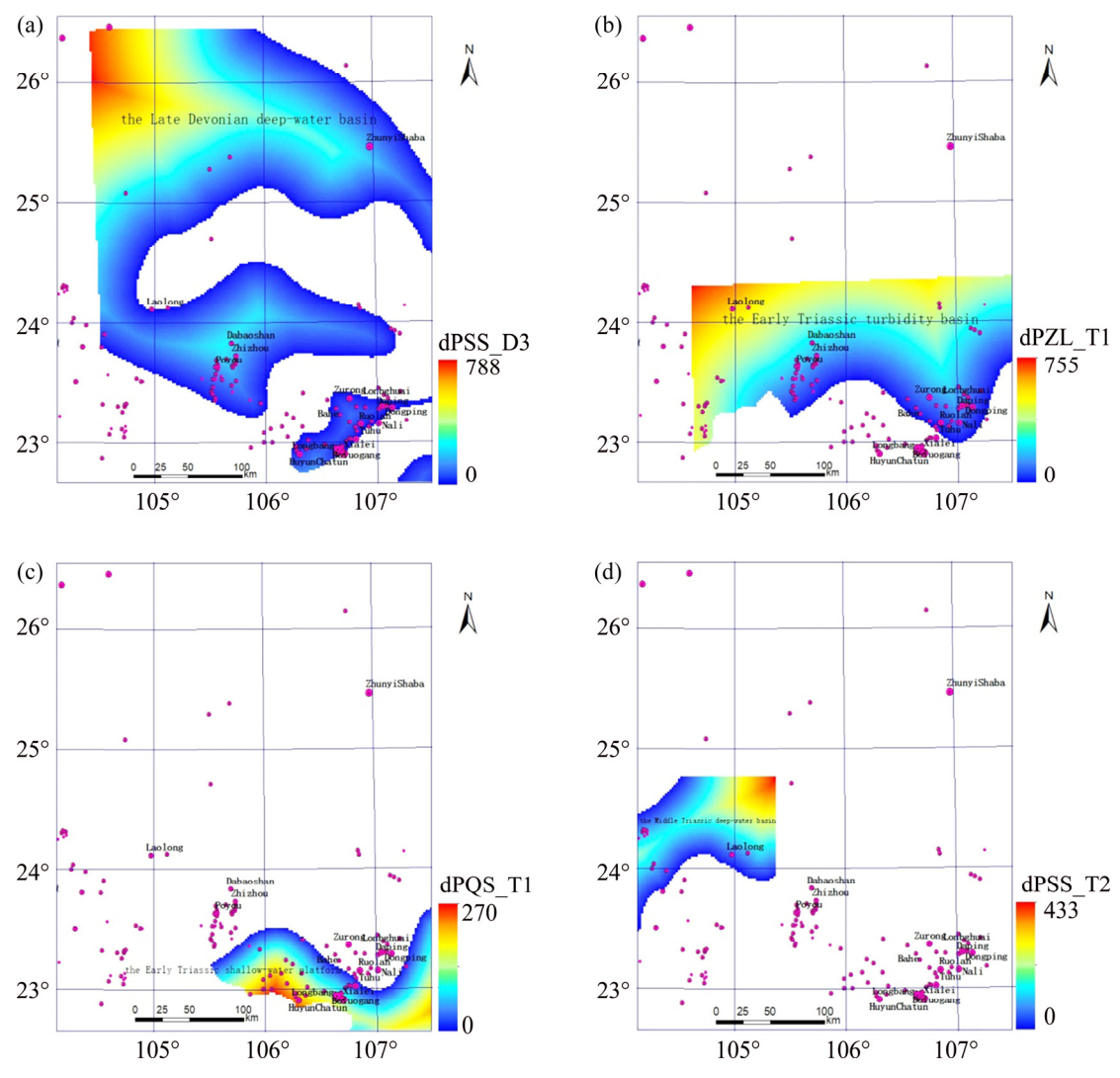


Fig. 2 Control field for synsedimentary faults: (a) Distribution of fF\_D3 for Middle Triassic; (b) Distribution of fF\_T2 for Late Devonian



**Fig. 3** Predictor maps of Euclidean distance field: (a) Late Devonian deep-water basin distance field dPSS\_D3; (b) Early Triassic turbidity basin distance field dPZL\_T1; (c) Early Triassic shallow-water platform distance field dPQS\_T1; (d) Middle Triassic deep-water basin distance field dPSS\_T2

facies gXAF D2, (2) the Late sedimentary Devonian Frasian sedimentary facies gXFL\_D3, (3) the Late Devonian Famennian Sedimentary facies gXFM D3, (4) the Middle Devonian Eifelian facies gXGFAF\_D2 Sedimentary in Funing. Guangxi, (5) the Middle Devonian Giverite facies gXGFAF\_D2 Sedimentary in Funing, Guangxi, and (6) the Middle Triassic Ladinian sedimentary facies gXLD T2. Here, sedimentary faces for each stage are encoded separately and assigned to the associated predictor variables.

#### 4.2.3.2 Topographical erosion degree

The trap and deposition of Mn metals are closely related to the topography and geomorphology conditions. The formation of

oxidized deposits is associated with the movement of surface and migration of groundwater. Thus, the topographical condition not only reflects the progress of erosion and accumulation, but also determines the dynamics of groundwater, and the state deposition and preservation of weathering products. The topographical surficial incision is adopted to represent the erosion degree. We use a DEM with a spatial resolution of 80 m to extract the surficial incision. The cutting degree refers to the difference between the average and minimum elevations in the neighborhood of a certain point on the ground. In the study area, the surficial incision ranges from 0 to 902 m. Figure 4 illustrates predictor map of the topographical erosion degree for the study area.

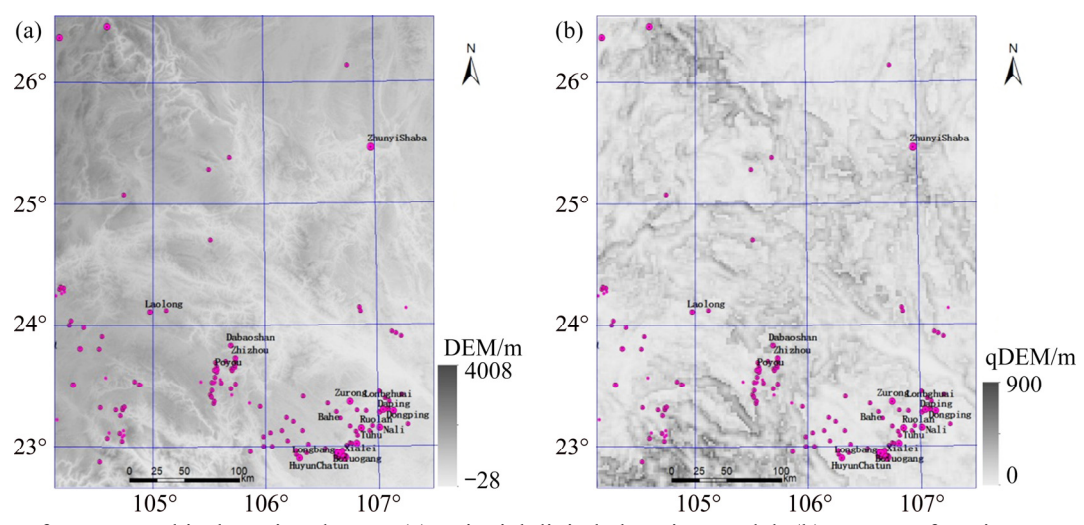


Fig. 4 Maps for topographical erosion degree: (a) Oringial digital elevation model; (b) Degree of cutting

#### 4.2.3.3 Lithology code

The lithologic association obtained from available geological data in WGSY region refers to 5 metallogenic stages, which corresponds to 5 predictor variables as follows: (1) the Middle Devonian Eifelian lithologic association gZAF\_D2, (2) the Middle Devonian Giverite lithologic association gZJW\_D2, (3) the Late Devonian Frasian lithologic association gZFL\_D3, and (4) the Late Devonian Famennian lithologic association gZFM\_D3. Here, each predictor variable is encoded separately according to the lithology association obtained in geological maps.

#### 4.2.3.4 Aeromagnetic anomalies

The Mn metal deposition can be reflected in the aeromagnetic anomalies, which is derived from the aeromagnetic  $\Delta T$  abnormal contour maps. To achieve the discretization of the map, the center point of each cell is spatially interpolated to obtain the aeromagnetic magnetic  $\Delta T$  values.

# 5 Modal-adaptive prospectivity modeling and mapping

#### 5.1 Modal-adaptive modeling approach

While the predictor variables defined in Subsection 4.2 provide a synthetic representation for the control to Mn deposits in WGSY region, the prospectivity modeling is still challenging due to information asymmetry between the known and unknown areas in the region. The information asymmetry lies in three aspects. Firstly, the significant difference in the geological and exploration work and the data inaccessibility lead to

an inconsistent degree in data completeness in the study area. That is, some predictor variables may be unavailable in certain areas. Secondly, since the geological process is heterogeneous in the region, the predictor variables may have different control ranges and valid predictor intervals between known and unknown areas. That is, some predictor variables may be invalid in unknown areas due to out of the actual control scope of associated geological features and the valid intervals learned from known areas. Given such issues information asymmetry, it is intractable to use a single prospectivity model for mapping of Mn potential in the entire region. Therefore, we develop modal-adaptive model specified for Mn prospecting in the WGSY region, which, instead of building a single prospectivity model, combines multiple models to adapt different areas of the region with diverse models of data collection and geological process.

Given n predictor variables, we can have different combinations of the variables according to the availability of predictor variables. To build the modal-adaptive models, we partition the study area into several scopes firstly with respect to different modals of data collection and geological process. To achieve the partition, we extract the valid scope for each predictor variable firstly, and then calculate the intersection of the valid scopes to obtain the final divided scopes. Accordingly, each scope  $S_i$  has one combination  $C_i$  of predictor variables that correspond to the available and valid predictor variables associated with the scope. Overall, we obtain m combinations of the predictor variables,

where m is the number of the partitioned scopes in WGSY region.

Given m combinations of predictor variables, we build a specialized prospectivity model for each combination according to the known deposits, which results in overall m models. Here, each model is built by using the Gaussian process regression (GPR) [30]. The Gaussian process is a stochastic process such that any finite collection of those random variables has a joint Gaussian distribution. The GPR assumes that a prior for the regression function f(x) of input x is generated from a joint Gaussian distribution over functions. Here, the joint Gaussian distribution has zero mean and covariance  $K(x_i, x_i) = \text{cov}(f(x_i), f(x_i))$  of the Gaussian form  $K(x_i, x_i) = A \exp\{-[(||x_i - x_i||^2)/(2h^2)]\}$ with amplitude A and bandwidth h. Under such an assumption, the Gaussian process prior for f can be written as p(f|x)=N(0, K), where K is the  $n \times n$  Gram matrix with element  $K_{ij} = \text{cov}(f(x_i), f(x_i))$ . On the other hand, let us assume that the input data x and the output variable y in the regression are generated following  $y=f(x)+\epsilon$ , where  $\epsilon$  denotes the Gaussian noise. The likelihood function p(y/f) for y can be formulated in a Gaussian from as  $p(y/f)=N(f,\sigma^2 I)$ , where I is the identity matrix. Finally, the marginal distribution of y can be obtained by combining the Gaussian process prior and the likelihood function:

$$p(y \mid X) = \int p(y \mid f) p(f \mid X) df = N(0, K + \sigma^2 I)$$
 (4)

With the posterior distribution as Eq. (4), we can easily derive the expected value of  $y^*$  for a new input  $x^*$  by conditioning the joint posterior distribution  $p(y,y^*|X,x^*)$  into  $p(y^*|X,y,x^*)$  [31]:

$$\hat{\mathbf{y}}^* = \mathbf{k}^{*T} (\mathbf{K} + \sigma^2 \mathbf{I})^{-1} \mathbf{y}$$
 (5)

where  $\hat{y}^*$  denotes the expected value that is the output variable of GPR, and  $k^*$  is the vector staking the covariance of  $K(x^*,x_i)$ .

Note that in the obtained combinations, some variable combinations are the subset of the other combinations. In other words, some scopes with a bigger set of predictor variables are associated with multiple prospective models which may be related to multiple metallogenic conditions and geological processes. Thus, we further combine the prospective models for these scopes instead of relying on a single model, which allows more flexibility in the adaptation of diverse modals of geological process. To achieve the combination, we

adopt the mixture of GPR models. Given l GPR models associated with a certain scope, each of which is associated with a Gaussian process  $p_i(y_i|X_i)$ , the mixture of distribution is formulated as follows:

$$\tilde{p}(\mathbf{y} \mid \mathbf{X}) = \sum_{i=1}^{l} \mu_i p_i(\mathbf{y} \mid \mathbf{X})$$
 (6)

where  $\mu_i$  denotes the mixture coefficients, and  $p_i(y|X)$  denotes the posterior distribution for each GPR model. To determine the hyperparameters  $\mu_i$ , we use a maximum likelihood approach which is analogous to the estimation of the mixture parameters of the famous Gaussian mixtures model [32]. Finally, in the same fashion as in Eq.(5), the output variable of y for the mixture model is obtained by conditioning the joint posterior distribution  $\tilde{p}(y^*, y|X, x^*)$  into  $\tilde{p}(y^*|X, y, x^*)$ 

$$\hat{y}^* = \sum_{i=1}^{l} \mu_i k_i^{*T} (K_i + \sigma^2 I)^{-1} y_i$$
 (7)

where the subscript i is used to distinguish the variables corresponding to different mixture model likewise in Eq. (6).

#### 5.2 Prospectivity mapping

For mapping of Mn prospectivity in WGSY, we divide the entire region into a set of cells. The resolution of the cell is set to 2 km × 2 km, resulting in 44298 cells for the study area. We calculate the predictor variables described in Section 4 for each cell and assign Mn mineralization information (Mn tonnage) to the cells in the known area. And then the modal-adaptive prospectivity modeling approach presented in Subsection 5.1 is adopted to build the prospectivity models for the study area by giving the cells in the known area. Because of different data availability and geological process, a total of 14 modal-adaptive prospectivity models have been built. With the prospectivity models, the prospectivity for each cell is obtained, resulting in a prospectivity map (Fig. 5) indicating Mn potential throughout the WGSY region.

The prospectivity map illustrated in Fig. 5 confirms the significant potential for Mn mineralization in the WGSY region. Several areas of high prospectivity have been identified although a missing of predictor variables. It is observed that the most prospective areas are closely associated with synsedimentary faults and located in sedimentary basins.

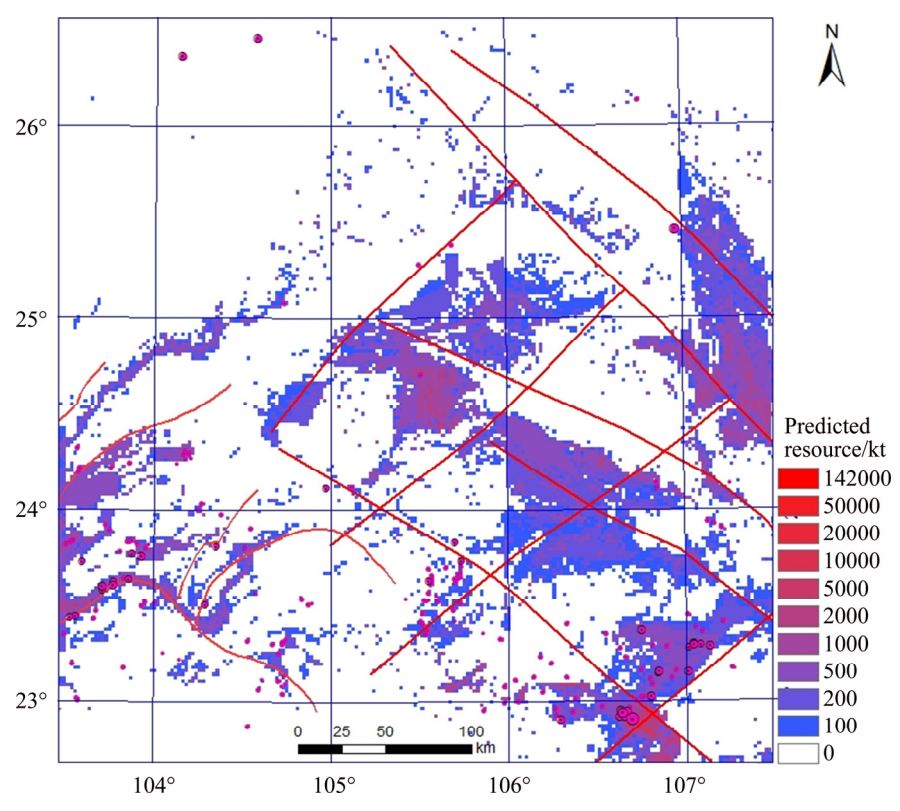


Fig. 5 Mn prospectivity map for WGSY region

According to the predictive Mn resources, the entire potential area is divided into 10 intervals that represent different levels of Mn prospectivity. There are 149 out of 175 known deposits that are inside the intervals corresponding to their known tonnage. Thus, the success rate is 85.1% for our modal-adaptive prospectivity models, which demonstrate the effectiveness of the spatial analysis and the modal-adaptive prospectivity modeling.

Specifically, the areas inside the 10th division of prospectivity, which may be prioritized for further exploration targeting, occupy 0.5% of the total prospective area in the WGSY region. Such highly prospective areas are mainly concentrated in two areas, that is, the area throughout Longbang-Xialei-Tuhu and the one throughout Yanzijiao-Dounan-Pucao-Taipingzhai. The former has an area of about 1111.1 km<sup>2</sup> and the predicted resource is 325.4×10<sup>6</sup> t (of which the known resource is 188.4×10<sup>6</sup> t). The main Mn-forming period of the area is the Late Devonian with the Mn-bearing strata of Upper Devonian Wuzhishan Formation (D<sub>3</sub>w) and the Dujiang Formation (D<sub>3</sub>l), whilst the favorable sedimentary facies lie in the syncline phase (II<sub>6</sub>) and foreslope facies (II<sub>5</sub>) areas of the platform. The thickness of the strata is large in the

middle of the area and gradually thins to the northeast and southwest. These characteristics reflect a close relation between the faulted tectonic setting of the Mn-bearing basin and the transitional extensional oceanic crust. The formation of Mn deposits in Late Devonian was controlled by a unified tectonic-magmatic thermodynamic field. The Funing-Daxin fault in the area, as an important extension of the synsedimentary faults, due to a likely linkage to the mantle, is deemed as the center of the source of energy and materials for Mn mineralization. On the other hand, the other prospective area has an area of 1401.8 km<sup>2</sup> and the predicted resource is 99.4×10<sup>6</sup> t (the known resource is  $42 \times 10^6$  t). The main Mn-forming period in this prospective area is the Middle Triassic Latin Nickel period, and the Mn-bearing stratum corresponds to the Middle Triassic Falang group  $(T_2f)$ . The deposits were mainly formed in a shallow sea and semi-restrict platform, which were mostly related to local depressions. Therefore, the mineralization in this area was controlled by the paleo-tectonic environment. The Mn favorable area is distributed along the Mingsu fault in a strip direction and extending to the intersection to the Wenma fault and the Zhuchang fault. The

intersection of the northwestern-trending paleofaults constrains the hot spring activity, which implies that the fault intersection in the submarine rift basin is of high probability for forming Mn deposits.

#### **6 Conclusions**

- (1) The Mn prospectivity modeling frameworks are tailored to adapt to regional scale Mn prospecting WGSY region. The spatial analysis approaches are specialized to extract prospectivity variables that effectively indicate the Mn mineralization. Specifically, to represent the metallogenic controls of the source of metals, the metallogenic fields are carefully designed for the quantification of the regional impact synsedimentary faults. Last but not least, to take the asymmetry of metallogenic information in integration of the predictor variables for regional Mn prospecting, a modal-adaptive model is proposed for Mn prospecting that allows to adapt not only different data modals to be integrated but also different geological processes to be quantified in the final prospectivity model.
- (2) The Mn prospecting workflow and the prospectivity mapping results for the WGSY region are presented, which range from the mineral system approach for deriving predictor variables to the final delineation of new prospectivity areas. The results demonstrate the effectiveness of the presented Mn prospectivity modeling frameworks in not only identifying known Mn deposits but also highlighting areas of high prospectivity.
- (3) The prospectivity mapping confirms the significant potential for discovering new Mn deposits in the WGSY region. The two areas throughout Longbang–Xialei–Tuhu and Yanzijiao–Dounan–Pucao–Taipingzhai respectively are highlighted as high priority targets for future mineral exploration. Efforts for district-scale exploration are suggested in these areas, especially the acquisition of new geological data of higher resolution to augment the district-scale prospectivity mapping.

#### References

[1] FU Yong, XU Zhi-gang, PEI Hao-xiang, JIANG Ran. Study on metallogenic regularity of manganese ore deposits in China [J]. Acta Geologica Sinica, 2014, 88(12): 2192–2207.

- [2] FAN De-lian, YANG Pei-ji. Introduction to and classification of manganese deposits of China [J]. Ore Geology Reviews, 1999, 15(1-3): 1-13.
- [3] YIN Jiang-ning, XIAO Ke-yan. Resources potential analysis and the metallogenic prospect of Mn resources in China [J]. Geology in China, 2014, 41(5): 1424–1437.
- [4] CONG Yuan, DONG Qin-ji, XIAO Ke-yan, CHEN Jian-ping, GAO Yong-bao, YIN Jiang-ning. Characteristics and predicted potential of Mn resources in China [J]. Earth Science Frontiers, 2018, 25(3): 118–137.
- [5] RAINES G L. Evaluation of weights of evidence to predict epithermal-gold deposits in the Great Basin of the Western United States [J]. Natural Resources Research, 1999, 8(4): 257-276.
- [6] GONZÁLEZ-ÁLVAREZ I, PORWAL A, BERESFORD S W, MCCUAIG T C, MAIER W D. Hydrothermal Ni prospectivity analysis of Tasmania, Australia [J]. Ore Geology Reviews, 2010, 38: 168–183.
- [7] XIAO Ke-yan, LI Nan, PORWAL A, EUN-JUNG H, LEON B, LU Yong-jun. GIS-based 3D prospectivity mapping: A case study of Jiama copper-polymetallic deposit in Tibet, China [J]. Ore Geology Reviews, 2015, 71: 611–632.
- [8] ZUO Ren-guang, CARRANZA E J M. Support vector machine: A tool for mapping mineral prospectivity [J]. Computers & Geosciences, 2011, 37(12): 1967–1975.
- [9] YOUSEFI M, CARRANZA E J M. Fuzzification of continuous-value spatial evidence or mineral prospectivity mapping [J]. Computers & Geosciences, 2015, 74: 97–109.
- [10] CHEN Yong-liang, WU Wei. Mapping mineral prospectivity using an extreme learning machine regression [J]. Ore Geology Reviews, 2017, 80: 200–213.
- [11] LIU Yue, ZHOU Ke-fa, ZHANG Nan, WANG Jin-lin. Maximum entropy modeling for orogenic gold prospectivity mapping in the Tangbale—Hatu belt, western Junggar, China [J]. Ore Geology Reviews, 2018, 100: 133–147.
- [12] XIONG Yi-hui, ZUO Ren-guang, CARRANZA E J M. Mapping mineral prospectivity through big data analytics and a deep learning algorithm [J]. Ore Geology Reviews, 2018, 102: 811–817.
- [13] TORPPA J, NYKÄNEN V, MOLNÁR F. Unsupervised clustering and empirical fuzzy memberships for mineral prospectivity modelling [J]. Ore Geology Reviews, 2019, 107: 58–71.
- [14] LI Sheng-fu, WANG Ze-hua, LI Lang-tian, XIA Liu-jing, JIAN Yao-guang, HOU Jian-sheng, CHEN Shi-xian. Analysis of the metallogenic mechanism of high-grade manganese ore in southwest Guangxi [J]. Resources Environment & Engineering, 2009, 23(4): 363–370.
- [15] LI Zhi-qun, LIANG Qiu-yuan, LIU Wen-jia, CHEN Ming-wei, ZOU Yun-da, ZHENG Rong-hua, GUO Xin. An analysis of sedimentary facies of manganiferous formation and manganese accumulation conditions in southeastern Yunnan [J]. Acta Geoscientica Sinica, 2013, 34(S1): s17–s24.
- [16] LUO Hua-bao. The direction of prospecting for high-quality manganese ore resources in China [J]. Geology and Prospecting, 2002, 38(4): 8–11.
- [17] XUE You-zhi, HOU Zong-lin. Geology and exploration of fine quality mn ore in china [J]. Contributions to Geology

- and Mineral Resources Research, 2006(S1): s1-s4.
- [18] HOU Zong-lin, XUE You-zhi, HUANG Jin-shui, LIN You-huan, LIU Hong-jun, YAO Jin-gu, ZHU Kai-jun. Manganese deposits related Yangtze platform [M]. Beijing: Metallurgical Industry Press, 1997: 1–364. (in Chinese)
- [19] HRONSKY J M A, GROVES D I. Science of targeting: Definition, strategies, targeting and performance measurement [J]. Australian Journal of Earth Sciences, 2008, 55(1): 3–12.
- [20] JOLY A, PORWAL A, MCCUAIG T C. Exploration targeting for orogenic gold deposits in the Granites-Tanami orogen: Mineral system analysis, targeting model and prospectivity analysis [J]. Ore Geology Reviews, 2012, 48: 349–383.
- [21] KNOX-ROBINSON C M, WYBORN L A I. Towards a holistic exploration strategy: using geographic information systems as a tool to enhance exploration [J]. Australian Journal of Earth Sciences, 1997, 44(4): 453–463.
- [22] KREUZER O P, ETHERIDGE M A, GUJ P, MCMAHON M E, HOLDEN D J. Linking mineral deposit models to quantitative risk analysis and decision-making in exploration [J]. Economic Geology, 2008, 103(4): 829–850.
- [23] WYBORN L A I, HEINRICH C A, JAQUES A L. Australian Proterozoic mineral systems: Essential ingredients and mappable criteria [C]//Proceedings of the AusIMM Annual Conference. Darwin, 1994: 109–115.
- [24] JOLY A, PORWAL A, McCUAIG T C. Mineral systems approach applied to GIS-based 2D-prospectivity modeling of geological regions: Insights from Western Australia [J]. Ore Geology Reviews, 2015, 71: 673–702.

- [25] HE Zhi-li. Study on genesis and perspective of some high quality manganese ore deposits in China [J]. Geotectonic et Metallogenia, 1990, 14(3): 203–210.
- [26] MAO Xian-cheng, ZENG Wen-bo, ZHOU Shang-guo, YAN Fang, DENG Ji-qiu, ZHANG Bao-yi. Research on relationship between digital terrain characteristics and spatial distribution of secondary enrichment manganese ore in western guangxi and south-eastern Yunan, SW China[J]. Geology and Exploration, 2009, 45(3): 292–298.
- [27] ZOU Yan-hong, LIU Yao, PAN Yong, YANG Kuan-da, DAI Ta-gen, MAO Xian-cheng, LAI Jian-qing, TIAN Hai-long. Numerical simulation of hydrothermal mineralization associated with simplified chemical reactions in Kaerqueka polymetallic deposit, Qinghai, China [J]. Transactions of Nonferrous Metals Society of China, 2019, 29: 165–177.
- [28] MOORE H. MATLAB for engineers [M]. Cambridge: Pearson, 2017.
- [29] JONES M W, BAERENTZEN J A, SRAMEK M. 3D distance fields: A survey of techniques and applications [J]. IEEE Transactions on Visualization and Computer Graphics, 2006, 12(4): 581–599.
- [30] GIBBS M N. Bayesian Gaussian processes for regression and classification [D]. Cambridge: University of Cambridge, 1998.
- [31] RASMUSSEN C E, WILLIAMS C K I. Gaussian processes for machine learning [M]. London: MIT Press, 2006.
- [32] BILMES J A. A gentle tutorial of the EM algorithm and its application to parameter estimation for Gaussian mixture and hidden Markov models [R]. U.C. Berkeley, 1998.

### 基于空间分析和模态自适应建模的 桂西—滇东南锰矿潜力制图

汪凡云 1,2, 毛先成 1, 邓 浩 1, 张宝一 1

- 1. 中南大学 地球科学与信息物理学院 有色金属成矿预测教育部重点实验室, 长沙 410083;
  - 2. 中南大学 出版社,长沙 410083

摘 要: 桂西一滇东南地区是我国著名的锰矿远景区,但由于地质因素的多样性、地质过程的复杂性和地质信息的不对称性,在该地区进行锰资源潜力制图具有挑战性。基于空间分析和模态自适应建模,对该地区锰矿资源潜力进行预测,为下一步找矿工作奠定基础。首先基于成矿系统方法,利用空间分析提取预测变量以识别地质过程特征;提出一种成矿场分析方法提取成矿信息,量化同沉积断裂和同沉积盆地的区域影响;在综合分析提取预测变量的基础上,建立适应不同数据可用性和地质过程的模态自适应预测模型。预测结果不仅与已知锰矿床分布具有高度的一致性,而且为今后的找矿工作提供了重要的参考。

关键词:资源潜力制图;锰矿;桂西一滇东南;场分析方法;模态自适应预测建模

(Edited by Wei-ping CHEN)